Nano Energy (2012) 1, 624–630

Available online at www.sciencedirect.com

SciVerse ScienceDirect

journal homepage: www.elsevier.com/locate/nanoenergy

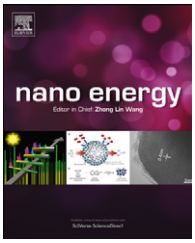

RAPID COMMUNICATION

Aromatic sulfide, sulfoxide, and sulfone mediated mesoporous carbon monolith for use in supercapacitor

Xiaochen Zhao[a,b,d], Qiang Zhang[a,c], Cheng-Meng Chen[a,d], Bingsen Zhang[a,e], Sylvia Reiche[a], Aiqin Wang[b], Tao Zhang[b,**], Robert Schlögl[a], Dang Sheng Su[a,e,*]

[a]*Department of Inorganic Chemistry, Fritz Haber Institute of the Max Planck Society, Faradayweg 4-6, Berlin 14195, Germany*
[b]*State Key Laboratory of Catalysis, Dalian Institute of Chemical Physics, Chinese Academy of Science, P.O. Box 110, Dalian 116023, PR China*
[c]*Beijing Key Laboratory of Green Chemical Reaction Engineering and Technology, Department of Chemical Engineering, Tsinghua University, Beijing 100084, PR China*
[d]*Graduate University of Chinese Academy of Science, Beijing 100049, PR China*
[e]*Shenyang National Laboratory for Materials Science Institute of Metal Research, Chinese Academy of Sciences, 72 Wenhua Road, Shenyang 110016, PR China*

Received 1 March 2012; received in revised form 23 April 2012; accepted 27 April 2012
Available online 9 May 2012

KEYWORDS
Sulfur;
Mesoporous carbon;
Supercapacitor;
Monolith

Abstract
Monoliths of aromatic sulfur mediated mesoporous carbon were fabricated via an aqueous self-assembly strategy and the species of sulfide, sulfoxide, and sulfone on the surface can be tuned rationally. The resultant S-doped mesoporous carbon exhibited superior performance as supercapacitor electrodes. The controllable modulation of sulfur species provided a possibility to clearly understand the role sulfur playing and allowed mechanistic insight into material requirements for high performance capacitors.

Introduction

Functionalization of heteroatoms at the edges, defects or strained regions of graphene geometries has been proven to be an efficient and effective way to tune the intrinsic chemical and electrical properties of carbon. Especially modified with heteroatoms, such as O, N, B, P, and S,

*Corresponding author at: Department of Inorganic Chemistry, Fritz Haber Institute of the Max Planck Society, Faradayweg 4-6, Berlin 14195, Germany. Tel.: +49 30 8413 4640; fax: +49 30 8413 4401.
**Corresponding author. Tel.: +86 411 84379015; fax: +86 411 84691570.
E-mail addresses: taozhang@dicp.ac.cn (T. Zhang), dangsheng@fhi-berlin.mpg.de (D. Sheng Su).

2211-2855/$ - see front matter © 2012 Elsevier Ltd. All rights reserved.
http://dx.doi.org/10.1016/j.nanoen.2012.04.003

showed promising performances in catalysis and electrochemical process [1]. For instance, heteroatoms (such as B and P) increase the selectivity in oxidative dehydrogenation (ODH) reactions on nanocarbons, which describes an attractive alternative to metal oxide catalysts for ODH of light alkanes [2]; Grafting sulfonates as acidic sites, or amino groups as basic sites revealed high performance in catalyzing the transesterification reaction in biomass conversion [3]; Nitrogen-doped carbons and/or graphitic carbon nitride presented high activity in liquid-phase ODH of dihydroanthracene to anthracene, and in photocatalysis [4]. Successful catalysis and electrochemical application of heteroatom modified carbon requires the manipulation of heteroatom-containing functional groups, especially on a suitably prepared mesoscopic material allowing for efficient transport of reactants and electrons.

The surface of carbon materials is usually terminated by a variety of functional groups. Sulfur shares the chalcogen group with oxygen, and the functionalization with sulfur containing groups is expected to be an important way to tune carbon chemistry. Sulfur containing functional groups allow to mediate carbon chemistry in different ways depending on their oxidation states [5], and show potential applications in biomass conversion [3], heavy metal recovery [6], and supercapacitor [7]. Usually, when the carbon materials or their precursors react with H_2SO_4, sulfonate will be grafted on the surface [3]. Besides, other species such as sulfide, sulfoxide, and sulfone may also play insignificant roles in modifying the surface properties, especially when sulfur atom is bonded with benzene rings or shares with a conjugated planar ring system with delocalized π electron clouds instead of discrete alternating single or double bonds. Thus, controllable modification of carbon with aromatic sulfide, sulfoxide, and sulfone is expected to bring novel surface chemistry, properties, and applications of carbon materials.

We explored the idea of aromatic sulfide, sulfoxide, and sulfone mediated mesoporous carbon (MPC) for supercapacitors. The reason for selecting MPC is attributed to their large surface areas, and uniform, tunable pore sizes [8]. Furthermore, chemically derived MPC are intrinsically decorated by abundant defect sites, such as functional groups, distortions and rough surfaces deviated from planer graphene on the lateral surface and edges. These sites allow for frequent surface modifications by sulfur groups that may reversibly absorb anion/cation species for supercapacitor application.

Experimental

Synthesis of 4,4′-thioldiphenol derived mesoporous carbons (TMCs)

To prepare TMC-denoted S-containig mesoporous carbons, 3.3 g (0.03 mol) of resorcinol and 2.2 g (0.01 mol) of 4,4′-thioldiphenol (TDP) were dissolved in a solution containing 20.0 g of water, 20.0 g of ethanol and 5.0 g of F127 under magnetic stirring until the solution turned transparent. Then, 1.2 g of HCl (32 wt%) was added to the solution as a catalyst and stirred for 1 h. Later 5.0 g of formaldehyde (37 wt%) was added to the above solution and kept stirring for 0.5 h until it turned cloudy. The cloudy mixture was kept standing at room temperature and separated into two phases finally. Afterwards, the upper layer was discarded, while the lower one was kept standing for another 2 days at room temperature until it turned transparent again. The sol was cured at 85 °C for 2 days, and then carbonized in Ar atmosphere at 350 °C and 650 °C for 3 h, respectively, with a ramping rate of 2 °C min^{-1}. The final product is denoted as TMC0.2, where 0.2 represents the mol ratio of sulfur to benzene ring. Meanwhile, TMC0.4 bearing different S content was also prepared via the same method, by varying the amount of resorcinol and TDP to 1.1 and 4.4 g, respectively.

Synthesis of the oxidative derivatives of TMCs (o-TMCs)

2.0 g obtained TMCx was dispersed into a mixture of 60.0 mL methanol and 60.0 mL HCl (2.0 M). 28.0 g of hydrogen peroxide (35 wt%) were added to the solution and kept stirring for 24 h at the temperature of 40 °C. The mixture was then filtered in vaccum and washed with deionized water several times until a neutrulized solution was obtained. The recovered material was dried at 110 °C overnight and designated as o-TMCx.

Characterization

Nitrogen sorption measurements were performed at −196 °C on a Micromeritics 2375 apparatus to determin the BET surface area and pore size distribution of these materials. X-ray diffraction (XRD) patterns were collected to investigate the ordering of mesopores on a PW3040/60 X' Pert PRO (PANalytical) diffractometer. A continuous mode was used for collecting data in the 2θ range from 0.5 to 4.5°. TEM images were obtained on a Philips CM200 LaB_6 microscope operated at 200 kV, while SEM as well as energy dispersive X-ray spectroscopy (EDS) was conducted on an FEI Quanta 200 FEG operated at 20.0 kV. A FEI C_s-corrected Titan 80-300 microscope was employed to acquire HAADF-STEM and elemental maps. The bulk S contents were determined by inductively coupled plasma atomic emission spectrometry (ICP-AES) on an IRIS Intrepid II XSP instrument (Thermo Electron Corporation). TG-MS analysis was conducted on a thermal gravimetric analysis (TGA) system comprising a TGA STA-449 Netsch apparatus equipped with a mass spectrometer (Pferffer Omnistar, Avi applied vacuum GmbH) as a detector under argon atmosphere. To reveal the surface properties, X-ray photoelectron spectroscopy (XPS) was conducted on ESCALAB250 (Thermo VG Corporation) equipped with a Al K_α radition (1486.6 eV, 15 kV, 10 mA, 150 W). Prior to fitting, a Shirley background was substracted. All binding energies (BEs) were corrected by charging of the samples by calibration on the graphitic carbon C1s peak at BE of 285 eV as a reference. The recorded spectra were fitted by a least square procedure to a product of Gaussian–Lorentzian functions. The concentration of each element was calculated from the area of the corresponding peak calibrated with the atomic sensitivity factor using C as reference.

Electrochemical measurement

For preparing a working electrode, a mixture of an active material, carbon black and poly(tetrafluoroethylene) (PTFE) with a weight ratio of 90:5:5 was ground together to form a homogeneous slurry. The slurry was squeezed into a film and then punched into pellets with a surface area of 1 cm^2 and weight of around 10 mg for each piece. The punched pellets with nickel foam on each side was pressed under 3 MPa and dried overnight at temperature of 110 °C. Prior to the electrochemical tests, the electrodes were impregnated with electrolyte under vacuum for 2 h. The cyclic voltammetry (CV) tests, Galvanostatic charge-discharge measurement (GC), and electrochemical impedance spectroscopy (EIS) profiles were performed on a VSP BioLogic potential workstation in a three-electrode cell in which a platinum slice was used as the counter electrode, a reverse hydrogen reference electrode (RHE) as the reference electrode and a 6 M KOH solution as the electrolyte. A scan rate from 2 mV s^{-1} to 100 mV s^{-1} and a current of 1 A g^{-1} were applied respectively in CV and GC studies. The Nyquist plot was original data without any fitting.

Results and discussion

Our concept involves a facile aquesous self-assembly coupled with carbonization strategy. In a typical process, TDP and resorcinol were employed as the carbon and sulfur precursors, respectively, and tri-copolymer F127 as the structure directing agent for polymerization (Figure 1a). The mixture of resorcinol and TDP polymerize with formaldehyde, and free hydroxyl groups in benzene rings could co-assemble with F127 via hydrogen bonds and form meso-structure [1,9]. Compared with pure resorcinol system, the combination with TDP decreased the reactivity towards formaldehyde, and thus provided an opportunity for the presence of methylol groups under acidic condition. These reactive methylol groups, in turn, may help the self-curing process via further condensation, transforming the sol into a gel, and finally form a monolith. However, this strategy decreased the amount of hydroxyl groups in the system, which can form hydrogen bonds with F127, thus induced a worm-like meso-structure without highly ordering. The resultant S-containing precursor was then carbonized under argon atmosphere at 650 °C to obtain TMCs with different S contents. To modulate the speciation and proportion of sulfoxide and sulfone, as well as aromatic sulfide, the as-obtained TMCs were treated with H_2O_2 in the presence of HCl, designated as o-TMCs. HAADF-STEM mapping (Figure 1b) and SEM-EDS mapping images (Figure S1) of o-TMC0.4 revealed a homogeneous distribution of elements S and O in the carbon.

TMC monolith was well preserved macroscopically after carbonization, and its size and shape is anticipated to be readily modulated by the mold in which hold their sol precursors (Figure S2). When the TMC monolith was observed by TEM, worm-like mesopores were detected in the TMCs (Figure S2). The pore texture was further evaluated by N_2 sorption isotherms. The typical type-IV profiles with well-defined H1 hysterises loops were characteristic of mesoporous structures and the narrow BJH distributions described well defined and uniform pore size of the TMCs

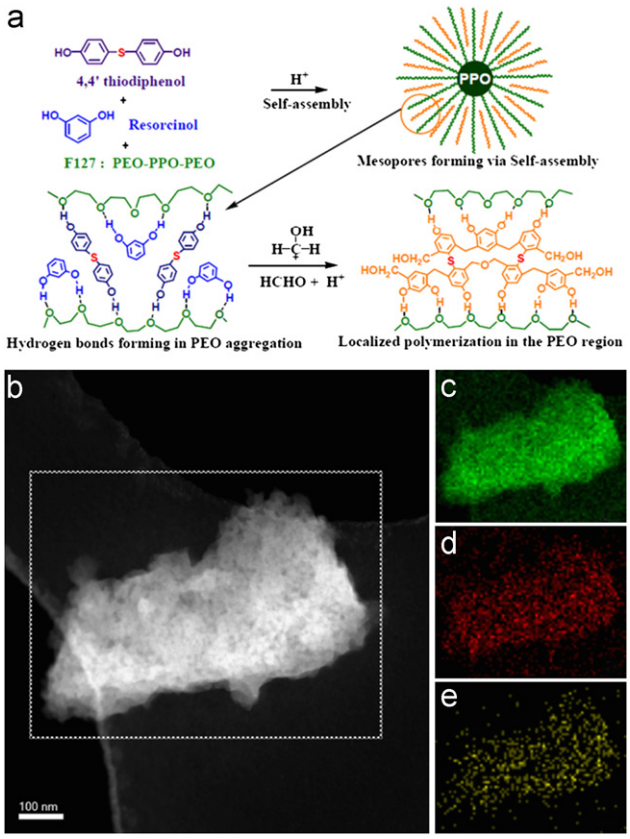

Figure 1 (a) Formation of aromatic sulfur mediated mesoporous carbon monolith by soft template polymerization. (b) HAADF-STEM of o-TMC0.4 and C, O, S mapping images.

(Figure S3). After H_2O_2 treatment, o-TMC monolith was obtained and the morphology of TMC was preserved, in spite of decreased BET surface area and average pore size. Table 1 summarized the textual parameters and elemental analysis results of the TMC and o-TMC samples. A decrease in the specific area and an increase in the pore size along with a broad distribution were presented when the S amount increased. This was attributed to the large employment of TDP, in which hydroxyl groups were shared by more beneze rings and hence disturbed the self-assembly for the lack of hydrogen-bonds forming component. However, one must bearing in mind that MPC was unavailable when pure TDP system without resorcinol addition was applied. In good agreement with N_2 sorption isotherms, the disapearence of reflection peak at around 0.7° in low-angle XRD patterns (Figure S3) indicated a deteriation of long range ordering with high content sulfur addition.

Since heteroatom functionalities tend to decompose under drastic pyrolysis condition, TG-MS method was employed in argon atmosphere to monitor the carbonization process, as well as sulfur species releasing. As shown in Figure 2, TMC0.4 and its precursor, 4,4′-thioldiphenol derived mesoporous polymer (TMP0.4) pyrolyzing at 350 °C, were selected as representative samples. A common feature for chemical derived carbonization was detected on the TG curve with a weight loss of 32% at *ca.* 600 °C (Figure 2a). Meanwhile, the substantial release of H_2S (m/z=34), SCO (m/z=60) and SO_2 (m/z=64) were attributed to the decomposition of incompletely

Table 1 Structural parameter and composition of TMCs and o-TMCs.

Sample	S_{BET} ($m^2\ g^{-1}$)	S_{meso} ($m^2\ g^{-1}$)	V_p ($cm^3\ g^{-1}$)	V_{meso} ($cm^3\ g^{-1}$)	D_p (nm)	S Cont. (wt%)
OMC	789	477	0.80	0.64	5.8	0
TMC0.2	732	416	0.80	0.63	6.3	0.49
TMC0.4	687	261	0.72	0.5	12.9	1.49
o-TMC0.2	662	378	0.62	0.48	6.2	0.54
o-TMC0.4	619	257	0.57	0.39	10.7	1.33

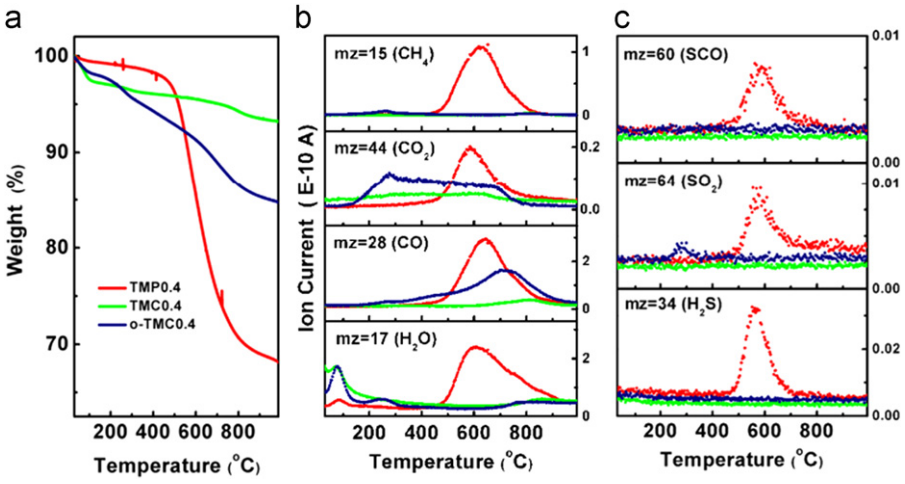

Figure 2 (a) TG and (b), (c) MS patterns of TMP0.4∗, TMC0.4 and o-TMC0.4. ∗ TMP is the polymer precursor of TMC, which was pre-pyrolysized at 350 °C to completely remove F127.

polymerized TDP fragments, unstable thiol groups, as well as their reaction with surface oxygen containing species. Clearly, all unstable sulfur groups decomposed below the temperature of 600 °C. Thus, the sulfur species comprised in TMCs are supposed tremendously thermally stable and are verified by the steady S-containing MS profiles of TMC0.4 (Figure 2c). In contrast, a small quantity of SO_2 was observed to desorb at approximate 270 °C for o-TMC0.4, indicating oxidized sulfur species were formed during the H_2O_2 treatment. Meanwhile, the liquid phase oxidation also yielded large amounts of carboxylic and anhydride groups on the surface (Figure 2b) [10]. Compared with TMC0.4, the extra 8.5% weight loss of o-TMC0.4 was attributed to these oxidized (or oxygen-containing) functional groups. However, the oxidation treatment modified merely the surface functional groups rather than the bulk and intrinsic properties. This was confirmed by the Raman spectroscopy (Figure S4), in which the intensity ratio of D1 (representing disordered graphitic lattice) to G (representing ideal graphitic lattice) bands (I_D/I_G) [11] maintained at the same level of 1.2 in both TMC and o-TMC samples.

To confirm the TG-MS results and further designate sulfur species, characterization with XPS was conducted on TMC0.4 and o-TMC0.4 (Figure 3). The sulfur (2p) spectra were split into three peaks mainly contributed by aromatic sulfide (164.1 eV [12]), sulfoxide (165.2 eV [12]), and sulfone (168.2 eV [12]). In TMC0.4, the sulfur existed mainly in the form of aromatic sulfide, whereas sulfoxide and sulfone species appeared as additional species in o-TMC0.4 with a 1:1 relative intensity. Combined with TG-MS results,

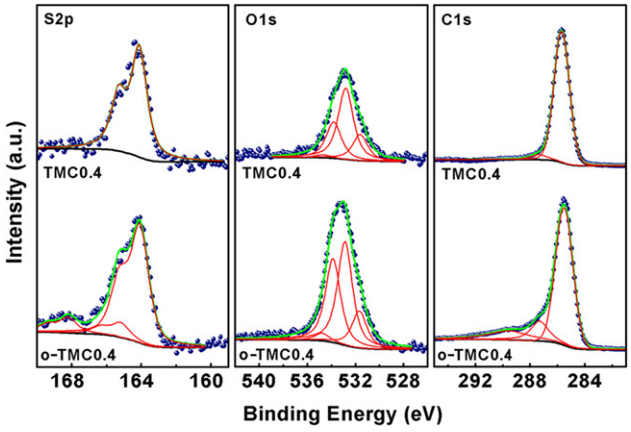

Figure 3 S2p, O1s and C1s spectra of TMC0.4 and o-TMC0.4. The blue dots are raw intensities, the green curves are sum intensities after fitting, the red splitted curves are fitting species.

aromatic sulfide speciation was convinced substantially stable under a pyrolysis at 1000 °C (more details in Figure S5 and Table S1), while sulfoxide or/and sulfone were responsible for the SO_2 evolution. Besides variation of sulfur species, the oxygen content increased from 5.8 to 12.4 wt% thanks to the H_2O_2 treatment (details in Table S1). In the O1s profiles, o-TMC0.4 displayed an upward trend of all

oxygen species, particularly of C-O (533.3 eV) and C-OH (534.2 eV) species [13]. Correspondingly, C1s XPS of o-TMC0.4 revealed increased peaks at 286.8 and 289.1 eV, assigned to C-O and C-OOH, respectively.

Supercapacitors are gaining increasing attention for complementing or replacing batteries in hybrid electric vehicles, portable electronics and industrial power management because of their large power density, moderate energy density, and longer cycle-life [14]. In order to evaluate the electrochemical energy-storage performance of the as-prepared materials, ordered mesoporous carbon (OMC), TMCs, and o-TMCs based electrodes for supercapacitors are fabricated. CV curves and GC profiles at low scan rate were provided to display an intrinsic performance of the obtained materials, while the calculated specific and gravimetric capacitance were shown in Figure 4, Figure S6 and Table 2. Since the surface area and surface chemistry are both significant factors for gravimetric capacitance, normalized specific capacitances, scanning at 2.0 mV s^{-1}, were provided in Figure 4a to minimize the influence of both structure and redox-related faradic response time. As exemplified by TMCs, the broadened charging-discharging curves suggested aromatic sulfide speciation as a positive function of capacitance. Though gained about 38% of specific capacitance, the CV shapes of TMCs were well preserved and no obvious peak was found comparing with S-free MPC. In sharp contrast, the shape

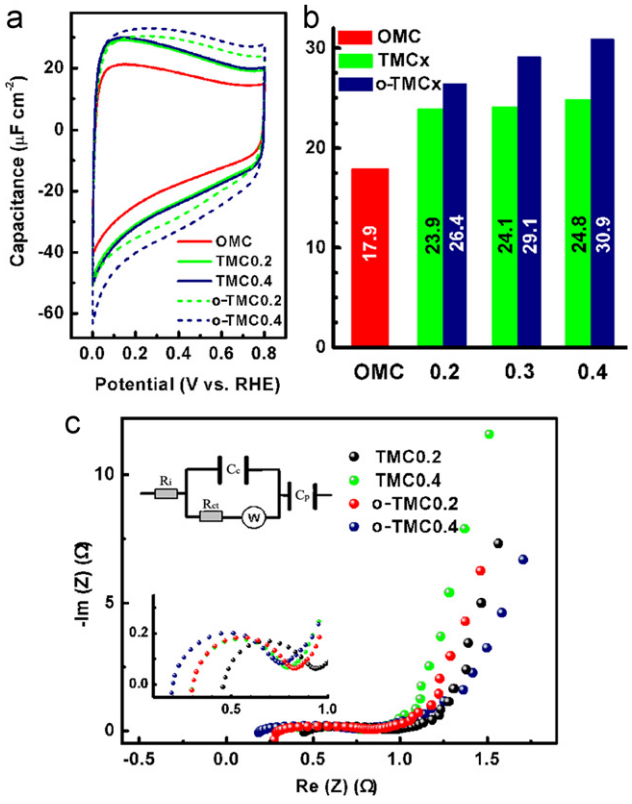

Figure 4 Electrochemical performance of TMCs: (a) CV curves in an alkaline electrolyte (6 M KOH); (b) Summarized Specific Capacitances of TMCs, o-TMCs and OMC. (c) AC impedance spectrums. This circuit comprises internal resistance (R_i), charge transfer resistance (R_{ct}) and capacitance (C_c), Warburg diffusion attributed to the ion migration through the electrode (Z_w) and the capacitance inside the pores (C_p).

Table 2 Capacitance of TMCs and o-TMCs and components of the equivalent circuit fitted for the impedance spectra.

Samples	C_s (μF cm^{-2})	C_g (F g^{-1})	R_i (Ω)	R_c (Ω)
OMC	17.9	142	0.44	1.02
TMC0.2	23.9	175	0.46	0.48
TMC0.4	24.8	170	0.31	0.48
o-TMC0.2	26.4	176	0.31	0.52
o-TMC0.4	30.9	191	0.20	0.57

of o-TMCs profiles varied greatly. Besides plateaus in CV curves, dissymmetric upward and downward of charging-discharging were observed as a function of sulfur content. Though the oxidation treatment of carbon contributes to the capacitance, the progressional widening of charging-discharging window along with the increase of sulfur revealed the insignificant role of oxidized S in improving the capacitance and required a different explanation for the performance of the o-TMC samples. The normalized capacitance achieved a further 14, 28, and 34% increase with introduction of sulfoxide and sulfone species in o-TMC0.2, o-TMC0.3, and o-TMC0.4, respectively (Figure 4b). Meanwhile, the galvanostatic charge-discharge (GC) results validated a same tendency (Figure S6).

To further interpret the kinetic behavior of the aromatic sulfide, sulfoxide, and sulfone mediated MPCs, electrochemical impedance spectroscopy (EIS) was studied in a frequency range from 10 kHz to 10 mHz, using an equivalent circuit [15] to simulate the capacitive and resistive element. The Nyquist plots of TMCs and o-TMCs electrodes (Figure 4c) showed a semicircle in the high frequency region followed by a sloping straight line. In the high frequency region, the intercept at the real impedance (Z') axis is related to the internal resistance (R_i), including the resistance of bulk electrolyte, intrinsic resistance of TMC or o-TMC materials and their contact resistance with Ni foam current collector. According to the parameters listed in Table 2, the R_i of all samples were below 0.5 Ω, illustrating a good conductivity of the testing system. With decreasing frequency, the semicircle emerge was caused by the charge transfer resistance (R_{ct}) at the interface between electrode and electrolyte. The minimum R_{ct} was recorded on TMC series materials (0.48 Ω) which were mainly doped with aromatic sulfide. This value gradually returned to 0.57 Ω (o-TMC0.4) after oxidation. Even though, compared with OMC (1.02 Ω), remarkable improvement of R_{ct} was achieved by the introduction of S species. In principle, R_{ct} represents an electrochemistry controlled process, while the following linear plots at low frequency reflected a diffusive resistivity of electrolyte ions within the pores. In Figure 4c, TMC0.2 and TMC0.4 displayed nearly vertical lines paralleling with each other, in spite of their marked differences in pore size and BET surface. This indicated ideal capacitive behaviors of TMCs, coordinating well with the CV curves, and ruled out the structure influence in this work. In contrast, the plots of o-TMCs inclined to a lower slope with increment of S content, suggesting higher diffusive resistance is produced due to the H_2O_2 treatment, particularly to the oxidation of S species.

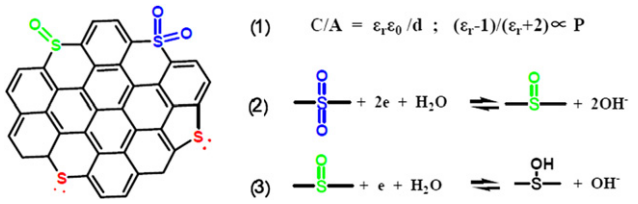

Figure 5 A proposed electrochemical performance mechanism on sulfur containing mesoporous carbon.

Several effects enhancing the supercapacitor performance with sulfur addition may be assumed (Figure 5). Firstly, more electron density is located at the surface of TMCs, thanks to a synergistic activation of conjugated carbon in combination with the electron-rich element S. Under an applied electric field, enhanced electric dipole moment enlarged the total polarization (*P*) of the medium [16]. According to equation (1) (Figure 5), the electrolyte dielectric constant (ε_r) multiplied with P and subsequently resulted in a superior normalized capacitance. Therefore, the increase of capacitance in TMC0.2 can be attributed to a larger ε_r and the charge transfer process is facilitated by the further polarization of the surface. Interestingly, instead of an increase with S content, the specific capacitance of TMCs maintained at a steady level with marginal improvement. This indicates that it is the presence of aromatic sulfide itself, rather than its concentration, that crucially modifies the enviroment of carbon surface. Secondly, a series of red-ox faradic reactions were carried out on o-TMCs at the additional sulfone and sulfoxide species. As illustrated in (2) and (3) in Figure 5, pseudo-capacitive properties are related with oxidized sulfur species and the capacitance is confirmed proportional to S content. Since the Faradaic process can be described in terms of charge-transfer resistance, the gradually increased R_{ct} of o-TMCs with S content is further explained. In brief, in the case of sulfur containing carbon, the introduction of n-type dopants S provides more polarized surface as well as reversible pseudo-sites and thus results in superior performance. Compared with oxygen [17], boron [2,18], nitrogen [3,17,19], or phosphorus [2,20] containing carbon, the sulfur containing functionalization is a facile, robust, representing promising way for novel active sites for enhanced capacitive performance.

Conclusion

In summary, a monolith of sulfur containing mesoporous carbon was obtained via a one-pot aqueous self-assembly synthesis strategy. These materials exhibit a uniform pore size (6 to 12 nm), a large surface area (about 700 $m^2\ g^{-1}$) and a controllable sulfur concentration between 0 and 1.5 wt% in the form of stable aromatic surfide groups. Further treatment of these materials with hydrogen peroxide modulates the ratio of aromatic sulfide, sulfoxide, and sulfone.The introduction of sulfur species, in particular of aromatic sulfur-containing groups, provided excellent supercapacitor performance. Compared with conventional ordered mesoporous carbon, TMC0.4 was improved by 20% in gravemetric and by 38% in specific capacitance, while o-TMC0.4 was improved by 34% and by 72%, respectively. This work disclosed a facile method to fabricate well-contolled sulfur-containing mesoporous carbons, with different chemical states of sulfur in tunable amounts. The trends in performance allowed mechanistic insight into the role sulfur playing for high performance supercapacitor and hence benefit the further heterogenerous catalysis and energy storage application.

Acknowledgments

The authors appreciate financial support by the EnerChem project of the Max Planck Society. The authors appreciate financial support of the National Basic Research Program of China (2009CB226102). The authors gratefully acknowledge Edith Kitzelmann, Frank Girgsdies, and Gisela Lorenz for experimental assistance and J.P. Tessonnier for fruitful discussion. X.C. Zhao and C.M. Chen also appreciate the sponsorship of the "Joint PhD Promotion Program 2010".

Appendix A. Supporting information

Supplementary data associated with this article can be found in the online version at http://dx.doi.org/10.1016/j.nanoen.2012.04.003.

References

[1] D.S. Su, J. Zhang, B. Frank, A. Thomas, X.C. Wang, J. Paraknowitsch, R. Schlogl, ChemSusChem 3 (2010) 169–180;
D.S. Yu, E. Nagelli, F. Du, L.M. Dai, Journal of Physical Chemistry Letters 1 (2010) 2165–2173;
J.H. Bitter, Journal of Materials Chemistry 20 (2010) 7312–7321;
X.C. Zhao, A.Q. Wang, J.W. Yan, G.Q. Sun, L.X. Sun, T. Zhang, Chemistry of Materials: a Publication of the American Chemical Society 22 (2010) 5463–5473;
D. Hulicova, M. Kodama, H. Hatori, Chemistry of Materials: a Publication of the American Chemical Society 18 (2006) 2318–2326.

[2] J. Zhang, X. Liu, R. Blume, A.H. Zhang, R. Schlogl, D.S. Su, Science (New York, NY) 322 (2008) 73–77;
B. Frank, J. Zhang, R. Blume, R. Schlogl, D.S. Su, Angewandte Chemie-International Edition 48 (2009) 6913–6917;
B. Frank, M. Morassutto, R. Schomacker, R. Schlogl, D.S. Su, ChemCatChem 2 (2010) 644–648.

[3] M. Toda, A. Takagaki, M. Okamura, J.N. Kondo, S. Hayashi, K. Domen, M. Hara, Nature 438 (2005) 178-178;
Q. Shu, Q. Zhang, G.H. Xu, Z. Nawaz, D.Z. Wang, J.F. Wang, Fuel Processing Technology 90 (2009) 1002–1008;
M. Hara, ChemSusChem 2 (2009) 129–135;
J.P. Tessonnier, A. Villa, O. Majoulet, D.S. Su, R. Schlogl, Angewandte Chemie-International Edition 48 (2009) 6543–6546;
Q. Shu, Z. Nawaz, J.X. Gao, Y.H. Liao, Q. Zhang, D.Z. Wang, J.F. Wang, Bioresource Technology 101 (2010) 5374–5384;
A. Villa, J.P. Tessonnier, O. Majoulet, D.S. Su, R. Schlogl, ChemSusChem 3 (2010) 241–245;
J.A. Macia-Agullo, M. Sevilla, M.A. Diez, A.B. Fuertes, ChemSusChem 3 (2010) 1352–1354.

[4] A. Thomas, A. Fischer, F. Goettmann, M. Antonietti, J.O. Muller, R. Schlogl, J.M. Carlsson, Journal of Materials Chemistry 18 (2008) 4893–4908;
X. Jin, V.V. Balasubramanian, S.T. Selvan, D.P. Sawant, M.A. Chari, G.Q. Lu, A. Vinu, Angewandte Chemie-International Edition 48 (2009) 7884–7887;

X.C. Wang, X.F. Chen, A. Thomas, X.Z. Fu, M. Antonietti, Advanced Materials (Weinheim, Germany) 21 (2009) 1609–1612.

[5] B.R. Puri, R.S. Hazra, Carbon 9 (1971) 123–134;
M. Nishioka, Energy and Fuels 2 (1988) 214–219;
J.M.J. Mateos, E. Romero, C.G. Desalazar, Carbon 31 (1993) 1159–1178.W.G. Feng, E. Borguet, R.D. Vidic, Carbon 44 (2006) 2990–2997.

[6] A. Macias-Garcia, C. Valenzuela-Calahorro, A. Espinosa-Mansilla, A. Bernalte-Garcia, V. Gomez-Serrano, Carbon 42 (2004) 1755–1764.

[7] G. Hasegawa, M. Aoki, K. Kanamori, K. Nakanishi, T. Hanada, K. Tadanaga, Journal of Materials Chemistry 21 (2011) 2060–2063.

[8] C.D. Liang, Z.J. Li, S. Dai, Angewandte Chemie-International Edition 47 (2008) 3696–3717;
J. Lee, J. Kim, T. Hyeon, Advanced Materials (Weinheim, Germany) 18 (2006) 2073–2094;
A.H. Lu, F. Schuth, Advanced Materials (Weinheim, Germany) 18 (2006) 1793–1805;
P. Gao, A. Wang, X. Wang, T. Zhang, Chemistry of Materials: a Publication of the American Chemical Society 20 (2008) 1881–1888.

[9] C.D. Liang, K.L. Hong, G.A. Guiochon, J.W. Mays, S. Dai, Angewandte Chemie-International Edition 43 (2004) 5785–5789;
S. Tanaka, N. Nishiyama, Y. Egashira, K. Ueyama, Chemical Communications (2005) 2125–2127;
Y.H. Deng, T. Yu, Y. Wan, Y.F. Shi, Y. Meng, D. Gu, L.J. Zhang, Y. Huang, C. Liu, X.J. Wu, D.Y. Zhao, Journal of the American Chemical Society 129 (2007) 1690–1697.

[10] J.H. Zhou, Z.J. Sui, J. Zhu, P. Li, C. De, Y.C. Dai, W.K. Yuan, Carbon 45 (2007) 785–796;
J.L. Figueiredo, M.F.R. Pereira, Catalysis Today 150 (2010) 2–7.

[11] A. Sadezky, H. Muckenhuber, H. Grothe, R. Niessner, U. Poschl, Carbon 43 (2005) 1731–1742.

[12] G.N. George, M.L. Gorbaty, S.R. Kelemen, M. Sansone, Energy and Fuels 5 (1991) 93–97;
M.A. Olivella, J.M. Palacios, A. Vairavamurthy, J.C. del Rio, F.X.C. de las Heras, Fuel 81 (2002) 405–411;
S.R. Kelemen, M. Afeworki, M.L. Gorbaty, M. Sansone, P.J. Kwiatek, C.C. Walters, H. Freund, M. Siskin, A.E. Bence, D.J. Curry, M. Solum, R.J. Pugmire, M. Vandenbroucke, M. Leblond, F. Behar, Energy and Fuels 21 (2007) 1548–1561.

[13] R. Arrigo, M. Havecker, S. Wrabetz, R. Blume, M. Lerch, J. McGregor, E.P.J. Parrott, J.A. Zeitler, L.F. Gladden, A. Knop-Gericke, R. Schlogl, D.S. Su, Journal of the American Chemical Society 132 (2010) 9616–9630.

[14] E. Frackowiak, F. Beguin, Carbon 39 (2001) 937–950;
D.S. Su, R. Schlogl, ChemSusChem 3 (2010) 136–168;
C. Liu, F. Li, L.P. Ma, H.M. Cheng, Advanced Materials (Weinheim, Germany) 22 (2010) E28–E62;
E. Raymundo-Pinero, M. Cadek, M. Wachtler, F. Beguin, ChemSusChem 4 (2011) 943–949;
M. Sevilla, S. Álvarez, T.A. Centeno, A.B. Fuertes, F. Stoeckli, Electrochimica Acta 52 (2007) 3207–3215;
A.B. Fuertes, G. Lota, T.A. Centeno, E. Frackowiak, Electrochimica Acta 50 (2005) 2799–2805;
V. Ruiz, C. Blanco, R. Santamaría, J.M. Ramos-Fernández, M. Martínez-Escandell, A. Sepúlveda-Escribano, F. Rodríguez-Reinoso, Carbon 47 (2009) 195–200.

[15] C.W. Huang, C.H. Hsu, P.L. Kuo, C.T. Hsieh, H.S. Teng, Carbon 49 (2011) 895–903;
G.H. Xu, C. Zheng, Q. Zhang, J.Q. Huang, M.Q. Zhao, J.Q. Nie, X.H. Wang, F. Wei, Nano Research 4 (2011) 870–881.

[16] K. Maex, M.R. Baklanov, D. Shamiryan, F. Iacopi, S.H. Brongersma, Z.S. Yanovitskaya, Journal of Applied Physics 93 (2003) 8793–8841;
J.S. Huang, B.G. Sumpter, V. Meunier, Angewandte Chemie-International Edition 47 (2008) 520–524.

[17] H.P. Boehm, Carbon 32 (1994) 759–769;
H.P. Boehm, Carbon 40 (2002) 145–149;
C.T. Hsieh, H. Teng, Carbon 40 (2002) 667–674;
D.S. Su, N. Maksimova, J.J. Delgado, N. Keller, G. Mestl, M.J. Ledoux, R. Schlogl, Catalysis Today 102 (2005) 110–114;
D. Hulicova-Jurcakova, M. Seredych, G.Q. Lu, T.J. Bandosz, Advanced Functional Materials 19 (2009) 438–447.

[18] D.W. Wang, F. Li, Z.G. Chen, G.Q. Lu, H.M. Cheng, Chemistry of Materials: a Publication of the American Chemical Society 20 (2008) 7195–7200.Y. Wang, J.S. Zhang, X.C. Wang, M. Antonietti, H.R. Li, Angewandte Chemie-International Edition 49 (2010) 3356–3359.

[19] W.R. Li, D.H. Chen, Z. Li, Y.F. Shi, Y. Wan, G. Wang, Z.Y. Jiang, D.Y. Zhao, Carbon 45 (2007) 1757–1763;
D. Hulicova-Jurcakova, M. Kodama, S. Shiraishi, H. Hatori, Z.H. Zhu, G.Q. Lu, Advanced Functional Materials 19 (2009) 1800–1809;
R.L. Liu, D.Q. Wu, X.L. Feng, K. Mullen, Angewandte Chemie-International Edition 49 (2010) 2565–2569;
D.S. Yu, Q. Zhang, L.M. Dai, Journal of the American Chemical Society 132 (2010) 15127–15129;
R.T. Lv, T.X. Cui, M.S. Jun, Q. Zhang, A.Y. Cao, D.S. Su, Z.J. Zhang, S.H. Yoon, J. Miyawaki, I. Mochida, F.Y. Kang, Advanced Functional Materials 21 (2011) 999–1006.

[20] D. Hulicova-Jurcakova, A.M. Puziy, O.I. Poddubnaya, F. Suarez-Garcia, J.M.D. Tascon, G.Q. Lu, Journal of the American Chemical Society 131 (2009) 5026–5027;
Y.J. Zhang, T. Mori, J.H. Ye, M. Antonietti, Journal of American Chemical Society 132 (2010) 6294–6295.